

Article

Kinetics of Non-Isothermal and Isothermal Crystallization in a Liquid Crystal with Highly Ordered Smectic Phase as Reflected by Differential Scanning Calorimetry, Polarized Optical Microscopy and Broadband Dielectric Spectroscopy

Małgorzata Jasiurkowska-Delaporte ^{1,*} , Tomasz Rozwadowski ^{1,2}
and Ewa Juszyńska-Gałązka ¹ 

¹ The Henryk Niewodniczanski Institute of Nuclear Physics, Polish Academy of Sciences, Radzikowskiego 152, 31-342 Kraków, Poland; Tomasz.Rozwadowski@ifj.edu.pl (T.R.); ewa.juszynska@ifj.edu.pl (E.J.-G.)

² Department of Chemistry, Faculty of Pure and Applied Sciences, University of Tsukuba, Tsukuba, Ibaraki 305-8571, Japan

* Correspondence: Malgorzata.Jasiurkowska-Delaporte@ifj.edu.pl; Tel.: +48-12-662-84-81

Received: 27 March 2019; Accepted: 10 April 2019; Published: 12 April 2019



Abstract: The kinetics of the non-isothermal and isothermal crystallization of the crystalline smectic B phase (soft crystal B, SmB_{cr}) in 4-n-butyloxybenzylidene-4'-n'-octylaniline (BBOA) was studied by a combination of differential scanning calorimetry (DSC), broadband dielectric spectroscopy (BDS) and polarized optical microscopy (POM). On cooling, part of the SmB_{cr} phase undergoes conversion to a crystalline phase and the remainder forms a glassy state; after the glass softens, crystallization is completed during subsequent heating. By analyzing the area of the crystal growing in the texture of SmB_{cr} as a function of time, the evolution of degree of crystallinity, $D(t)$, was estimated. It was demonstrated that upon heating, $D(t)$ follows the same Avrami curve as the crystallization during cooling. Non-isothermal crystallization observed during slow cooling rates ($3\text{K}/\text{min} \leq \phi \leq 5\text{K}/\text{min}$) is a thermodynamically-controlled process with the energy barrier $E_a \approx 175\text{ kJ}/\text{mol}$; however, the crystallization occurring during fast cooling ($5\text{ K}/\text{min} > \phi \geq 30\text{K}/\text{min}$) is driven by a diffusion mechanism, and is characterized by $E_a \approx 305\text{ kJ}/\text{mol}$. The isothermal crystallization taking place in the temperature range 274 K and 281 K is determined by nucleus formation.

Keywords: non-isothermal and isothermal crystallization processes; liquid crystals; differential scanning calorimetry; broadband dielectric spectroscopy; polarized optical microscopy

1. Introduction

Crystallization is defined as the formation of a solid phase with a long-range order composed of repeated units called unit cells. This intriguing phenomenon is commonly observed for various organic [1,2] and inorganic [3–5] systems upon cooling below their melting temperature (melt crystallization), which is in line with thermodynamics, i.e., Gibbs free energy is higher for the isotropic liquid than for a crystal. There is also a large group of materials which can be easily supercooled into a glassy state, from which so-called “cold” crystallization can be observed during heating, after softening of the glass. Despite intensive research efforts, the process of crystallization is a complex one and little is understood of its nature and control. Crystallization occurs through two inseparable steps [6], nucleation and crystal growth, and it is governed by the interplay between thermodynamic driving force and molecular mobility [7–10]. Transformation into the macroscopic crystal is possible

only if its constituent nuclei overcome the activation energy associated with their critical size [11]. This can be achieved by maintaining the sample within the optimal temperature range for nucleation and crystal growth (isothermal crystallization) or cooling it slowly enough to form a new phase (non-isothermal crystallization). The latter is of great importance in industrial processes, which often take place under non-isothermal conditions. Investigations of non-isothermal processes allow the temperature range of studies to be extended beyond that accessible to isothermal measurements. Both kinds of experiments are necessary to elucidate the full crystallization pattern of a material.

Crystallization is also observed for liquid crystals (LCs), which are characterized by a variety of mesophases with different degrees of ordering, and some demonstrate rich solid-state polymorphism [12]. It was found that the crystallization process in LCs is influenced by structure of the initial phase and thermal history of the sample. Although there are several scientific studies concerning the formation of three-dimensional (3D) crystalline solids from the nematic phase (N) [13–18], little attention is paid to crystallization from highly-ordered crystal-like smectic phases. An interesting example in this regard is the crystallization of the smectic B (SmB) phase in 4-n-butyloxybenzylidene-4'-n'-octylaniline (BBOA, also abbreviated as 4O.8). Calorimetric measurements found BBOA to possess a rich mesomorphism on heating [19]: Cr -310.5K - SmB -321.1K - SmA -335.3K - N-351.0K-I. Interestingly, upon cooling, an additional phase transition from the SmB_{hex} to the SmB_{Cr} phase (also called “soft crystal” [20]) was observed at 287 K [21]. X-ray experiments demonstrate that while both phases show a hexagonal arrangement of molecules within the smectic layer, they differ with regard to their molecular correlation length [22]. Broadband dielectric spectroscopy (BDS) studies indicate that the SmB_{hex} to the SmB_{Cr} transition is also characterized by retardation of the flip-flop rotation of molecules around their short axis accompanied by an increase of activation energy. Moreover, the SmB_{Cr} phase can vitrified if the substance is quenched or crystallized during very slow cooling.

The present paper describes a detailed study of the crystallization behaviour of SmB_{Cr} of 4-n-butyloxybenzylidene-4'-n'-octylaniline (BBOA) under isothermal and non-isothermal conditions using a combination of broadband dielectric spectroscopy (BDS), differential scanning calorimetry (DSC) and polarized optical microscopy (POM). To determine the mechanism of the crystallization process, the DSC data were analysed according to approaches proposed by Ozawa and Mo. The findings for the non-isothermal process were compared with those regarding isothermal crystallization obtained from BDS studies.

2. Materials and Methods

2.1. Material

The BBOA material was supplied from the Institute of Chemistry, Military University of Technology, Warsaw, Poland and used as received. The substance was synthesized according to the procedure outlined elsewhere [23]. The purity was determined to be better than 99.5% using the ASTM E928 Standard Test Method for Determining Purity by differential scanning calorimetry [24]. At the beginning of every measurement, the substance was heated up above melting temperature and was kept for 3 min to ensure complete melting.

2.2. Broadband Dielectric Spectroscopy (BDS)

To carry out BDS measurements, BBOA powder was heated to the isotropic phase between two circular electrodes with a diameter of 10 mm, which were separated by Teflon spacers to avoid a short circuit. The complex dielectric functions $\varepsilon^*(\omega) = \varepsilon'(\omega) - i\varepsilon''(\omega)$ were measured at the frequency range 0.1–10⁷ Hz by means of a high-precision dielectric analyzer (ALPHA analyzer; Novocontrol Technologies, Montabaur, Germany) at the selected temperatures. The sample temperature was stabilized with an accuracy better than 0.1 K by a Novocool temperature controller. Pure nitrogen gas was used as the heating agent.

2.3. Differential Scanning Calorimetry (DSC)

DSC measurements were performed for several cooling/heating rates for a 7.17 mg sample using a DSC 2500 Differential Scanning Calorimeter (TA Instruments, New Castle, Delaware, USA). Temperature modulated DSC (MDSC) measurements were taken with the DSC 2500 under a nitrogen atmosphere at a heating rate of 3 K min⁻¹ with a temperature modulation amplitude of 0.5 K and modulation period of 60 s.

2.4. Polarizing Optical Microscopy (POM)

The temperature evolutions of the textures were observed using a Biolar PI polarizing light microscope (PZO, Warsaw, Poland) in combination with a Linkam THM600 heating stage (Linkam Scientific Instruments, Tadworth, UK). The temperature of the sample was controlled with a high degree of accuracy (± 0.1 K) using a flow of liquid nitrogen. The thickness of the layer was about 50 μm . The degree of crystallinity $D(t)$ was determined by the graphical analysis of textures by means of GIMP graphics application software (open source). The growing crystalline phase regions were marked in black, whereas the remaining parts of the SmB_{Cr} phase were marked in white using the color curves tool in GIMP. The percentage cover of the whole texture layer by the crystalline area is provided in a colored histogram. The value of $D(t)$ is given by:

$$D(t) = \frac{S_{Cr}(t)}{S} \quad (1)$$

where $S_{Cr}(t)$ is the area of the texture related to the new Cr phase and S is the total surface area of the texture.

3. Results and Discussion

3.1. Non-Isothermal Crystallization Processes as Followed Using DSC and POM

To elucidate the tendency of BBOA to crystallize upon cooling under various conditions, the study first examined the kinetics of non-isothermal crystallization by means of DSC measurements at various cooling rates (see Figure 1a). Upon cooling, BBOA shows four mesophases with increasing degrees of molecular order: N-SmA-SmB_{hex}-SmB_{Cr} as confirmed by the texture analysis (Figure 1). Following this, the SmB_{Cr} phase undergoes partial crystallization while the remaining volume of the sample vitrifies. Upon subsequent heating at a rate of 5 K/min, a complex cold crystallization consisting of a broad exothermal peak with three maxima at around 241 K, 249 K and 261 K was observed in the metastable SmB_{Cr}; this shifted towards higher temperatures as the heating rate increased.

This finding supports those of earlier adiabatic calorimetry studies, which found that two metastable crystalline phases become transformed to a stable crystalline phase [19]. To obtain data equivalent to these adiabatic calorimetric findings, BBOA was measured in the modulated DSC mode (MDSC), which provides more information than conventional DSC experiments [25]. MDSC benefits from the fact that it calculates the kinetic component from the total heat flow and its heat capacity component. The total signal is equivalent to standard DSC; the reversing signal provides information on heat capacity and melting, while the non-reversing signal shows cold crystallization and crystal perfection. The non-reversing heat flow, illustrated by the green curve in Figure 1c, shows two well-separated anomalies at 241 K and 273 K, associated with cold crystallization, as well as a complex melting of the ordered crystal phase at about 310 K. The curve also shows less intense anomalies describing phase transitions between the SmA, N and I phases.

In contrast to the DSC measurements, the cold crystallization Figure 1b,c is a well-separated two-step process with a very intense and sharp peak at 241 K and a broader one at 273 K. The latter peak most likely describes an additional ordering of molecules. The anomaly at about 310 K, demonstrating an SmB-SmA phase transition, appears to be a separated two-step process (according to the non-reversing heat flow curve), while DSC measurements indicate an unresolved pair of anomalies

in the form of a single broad peak. The higher-temperature anomalies associated with the non-reversing heat flow, i.e., above 310 K, are not very intensive, in contrast to the analogous anomalies observed on the total heat flow. These anomalies correspond to phase transitions between mesophases with a characteristic ordering of SmA, N and I phases; the SmA and N phases show lack of any crystal ordering, i.e., they possess only orientational ordering, while the I phase does not display any ordering.

By integrating the crystallization peak of the DSC thermograms presented in Figure 1a, the relative degree of the non-isothermal crystallization (D) for each cooling rate can be determined as a temperature function [26]:

$$D(T) = \frac{\int_{T_0}^T \left(\frac{dH}{dT}\right) dT}{\int_{T_0}^{T_\infty} \left(\frac{dH}{dT}\right) dT} \quad (2)$$

Here, T_0 and T_∞ are temperatures at which the crystallization process respectively begins and ends, whereas dH/dT represents the heat flow at a given temperature T . To take into account the fact that only partial crystallization occurs upon cooling, and that the recrystallization of supercooled SmB_{cr} (cold crystallization) is then observed upon heating, the value determined from Equation (2) was multiplied by the ratio of the peak area obtained on cooling and heating. The temperature dependences of D are presented in Figure 2c. The degree of crystallization that was achieved upon cooling decreases with increasing cooling rate, from $D = 89\%$ ($\phi = 2$ K/min) to $D = 13\%$ ($\phi = 30$ K/min).

The growth of the crystal Cr from SmB_{cr} upon cooling was also monitored by polarized microscopy (POM) observations of the texture evolution as described in the experimental section. It is evident in Figure 2b,d that the crystalline centers grow equally in all directions and their number increases with decreasing temperature. The crystallization temperature T_c and crystallization characteristic time τ_{cr} determined using POM are in good agreement with the values obtained by DSC (Figure 2c).

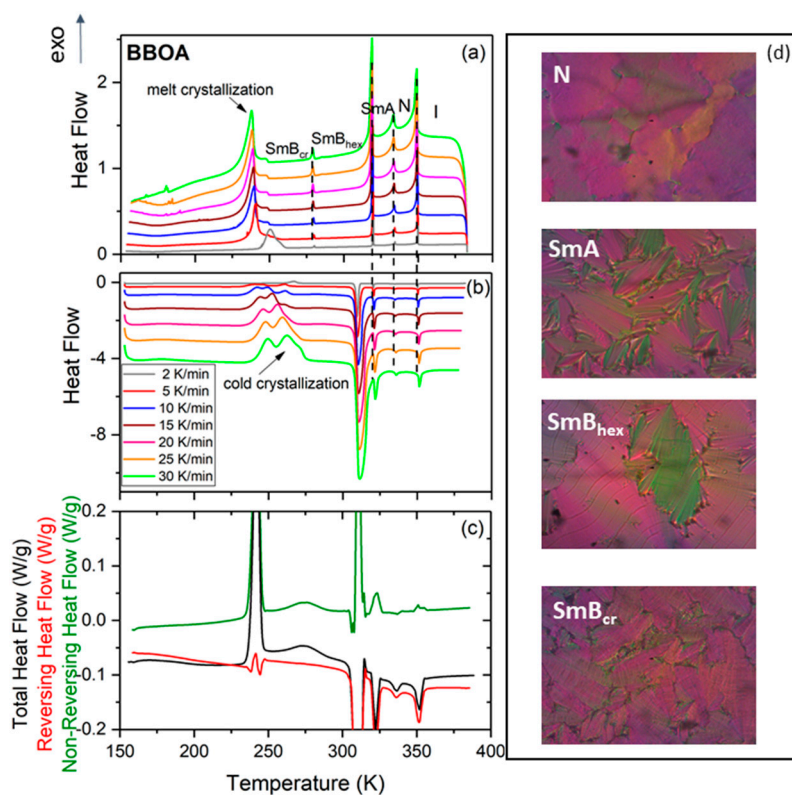


Figure 1. Differential scanning calorimetry (DSC) thermograms of 4-n-butyloxybenzylidene-4'-n'-octylaniline (BBOA) obtained at various rates of cooling (a) and heating (b). (c) MDSC thermogram of BBOA obtained for a heating rate 3 K min⁻¹ with a modulation amplitude of 0.5 K for a period of 60 s. (d) Exemplary textures of BBOA in various mesophases as indicated.

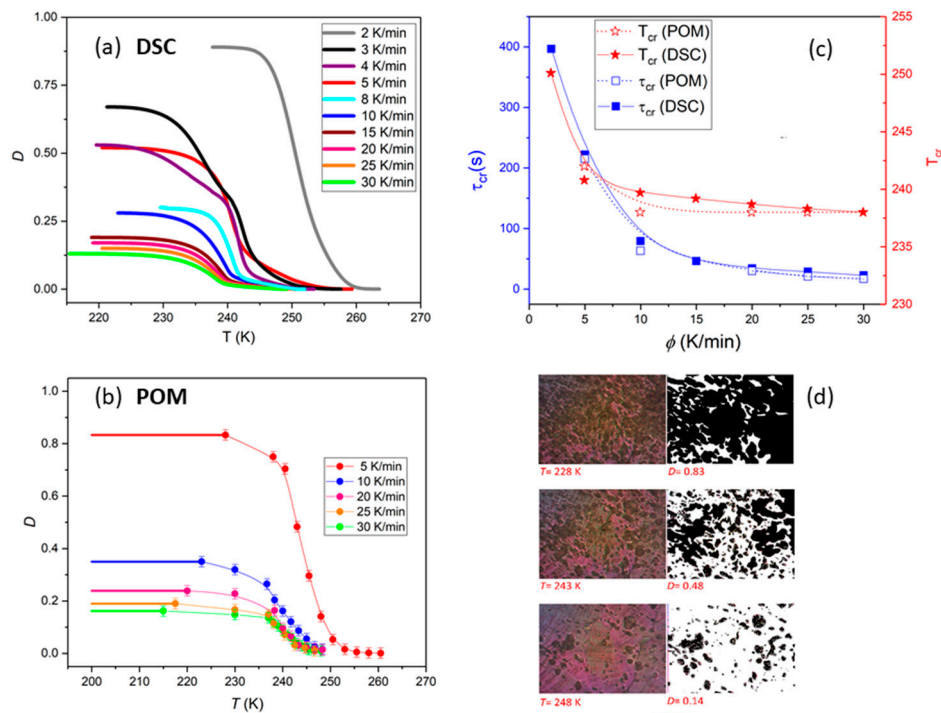


Figure 2. (a) Temperature dependences of the crystallization degree $D(T)$ determined from DSC measurements with different cooling rates ϕ . (b) Increase of degree of crystallinity with decreasing temperature obtained from the graphical analysis of the BBOA textures for various cooling rates. (c) Comparison of the crystallization temperature T_c and crystallization characteristic time τ_{cr} determined by DSC and polarized optical microscopy (POM) studies. τ_{cr} was assumed as time needed to achieve 63% of maximal crystallinity degree that was found upon cooling. (d) Evolution of textures during non-isothermal crystallization of the sample cooled down with the rate 5 K/min. The error bars are smaller than the symbols, if not explicitly stated otherwise.

Polarized microscopy was also used to study how the crystallization process is completed upon heating. The crystalline fraction can be seen to increase during cooling and then on subsequent heating (Figure 3). Interestingly, the change in the degree of crystallinity observed over time during heating follows the same Avrami curve as for the crystallization process occurring during cooling. It follows that total crystallization, not being restricted by the partial vitrification of the sample, would take the same time as the incomplete crystallization during cooling. Then, further changes in microscopic textures of the crystalline phase were observed, which indicated a transformation to a better ordered phase.

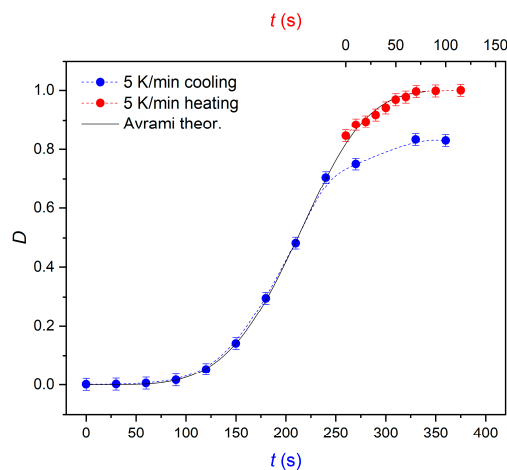


Figure 3. Time evolution of the crystallinity degree $D(t)$ observed by POM on cooling (partial crystallization) and heating at the rate of 5 K/min. The black line denotes the theoretically-predicted Avrami curve.

3.2. Analysis of Non-Isothermal Melt Crystallization Kinetics Observed by DSC

Activation energy E_c for the non-isothermal crystallization process was estimated using an equation proposed by Kissinger [27]:

$$\ln \frac{\phi}{T_p^2} = C - \frac{E_c}{RT_p} \quad (3)$$

and by Augis and Bennett [28]:

$$\ln \frac{\phi}{T_p - T_0} = C_{AB} - \frac{E_c}{RT_p} \quad (4)$$

where C and C_{AB} are fitting parameters, ϕ means a cooling/heating rate, T_p indicates the maximum crystallization peak and T_0 is the onset temperature of crystallization. Two different linear dependences were found for $3 \text{ K/min} \leq \phi \leq 5 \text{ K/min}$ and $5 \text{ K/min} > \phi \geq 30 \text{ K/min}$, indicating two different mechanisms of crystallization for slow and fast cooling (see Figure 4). The values of E_c estimated using both methods coincide and are approximately equal to 175 kJ/mol and 305 kJ/mol for the slow and fast cooling, respectively.

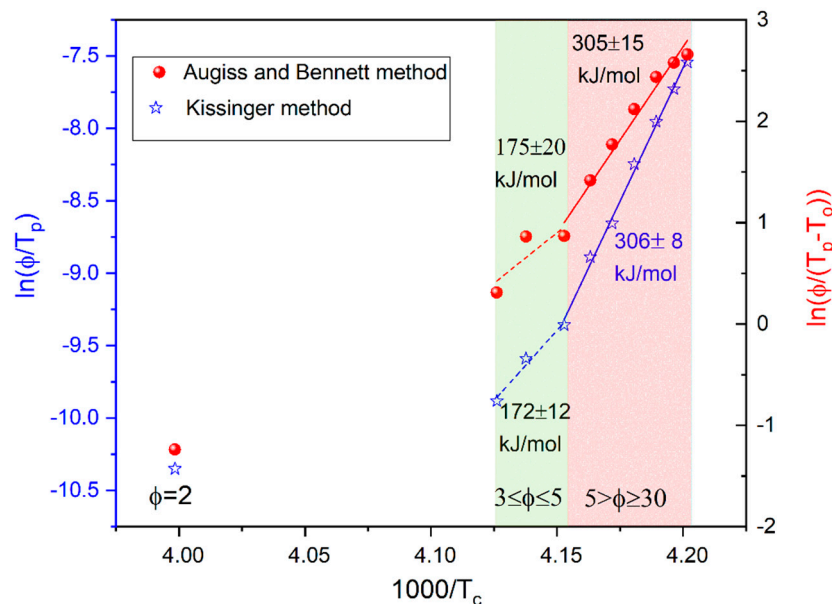


Figure 4. Kissinger (empty symbols) and Augis and Bennett (solid symbols) plots for the crystallization process observed for BBOA upon cooling.

In the first step, the mechanism of non-isothermal crystallization is studied according to Ozawa [29]. Assuming that the non-isothermal crystallization process consists of infinitesimally small isothermal crystallization steps, the time variable t in the Avrami model can be replaced with the quotient of temperature and heating rate T/ϕ , resulting in the following equation:

$$\log(-\ln(1-D)) = \log Z(T) - n_O \log(\phi) \quad (5)$$

where D is the relative degree of non-isothermal crystallization, n_O is the Ozawa exponent depending on the dimensionality of the crystal and $Z(T)$ is the Ozawa crystallization rate. It is evident in Figure 5 that the Ozawa analysis provides a good description of the non-isothermal crystallization of the BBOA SmB_{cr} phase only during cooling, with $\phi \geq 10 \text{ K/min}$. For fast cooling the plots of $\log(-\ln(1-D))$ versus $\log(\phi)$ yield a straight line with n_O being the slope and $\log(Z(T))$ the intercept with the y-axis. The value of $\log(Z(T))$ decreases with increasing temperature (Table 1), indicating that non-isothermal crystallization for fast cooling occurs in the diffusion-controlled region.

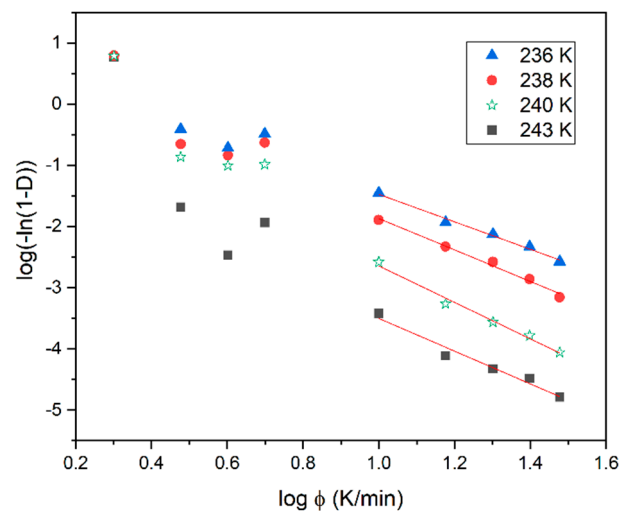


Figure 5. Ozawa plots based on the non-isothermal crystallization DSC data obtained for BBOA.

Table 1. Parameters of non-isothermal melt crystallization kinetics of BBOA obtained from the Ozawa analyses.

| Ozawa Model | | |
|-------------|-----------------|---------------------------------|
| T (K) | n_o | $\log(Z \text{ (K/min)}^{n_o})$ |
| 236 | 2.24 ± 0.12 | 0.77 ± 0.16 |
| 238 | 2.56 ± 0.14 | 0.69 ± 0.17 |
| 240 | 2.98 ± 0.19 | 0.34 ± 0.24 |
| 243 | 2.67 ± 0.28 | -0.82 ± 0.35 |

Additionally, the non-isothermal crystallization process was analyzed by the approach proposed by Mo et al. [30,31], which combines the Ozawa and Avrami equations as below:

$$\log Z(t) - n_o \log \phi = \log k + n_A \log t \quad (6)$$

$$\log \phi = \log F - a \log t \quad (7)$$

where a is the ratio of the Avrami exponent n_A (providing information on the type of nucleation and the dimensionality of crystal growth during isothermal experiment) to the Ozawa n_O exponent, $F = (Z/k)^{\frac{1}{n_O}}$ is related to the cooling/heating rate. Figure 6 presents the relationship between cooling rate and crystallization time for the fixed degree of crystallinity D . The dependence of $\log t$ ($\log \phi$) below 5 K/min is different to that above, as indicated by the slope. The $\log Z$ values increase as the fraction of the new phase (D) grows. Together, these findings support the idea that slow and fast cooling rates are associated with different mechanisms of crystallization; a similar pattern was previously observed for the crystallization of the nematic phase of 4-Cyano-3-fluorophenyl 4-Butylbenzoate (4CFPB) [15].

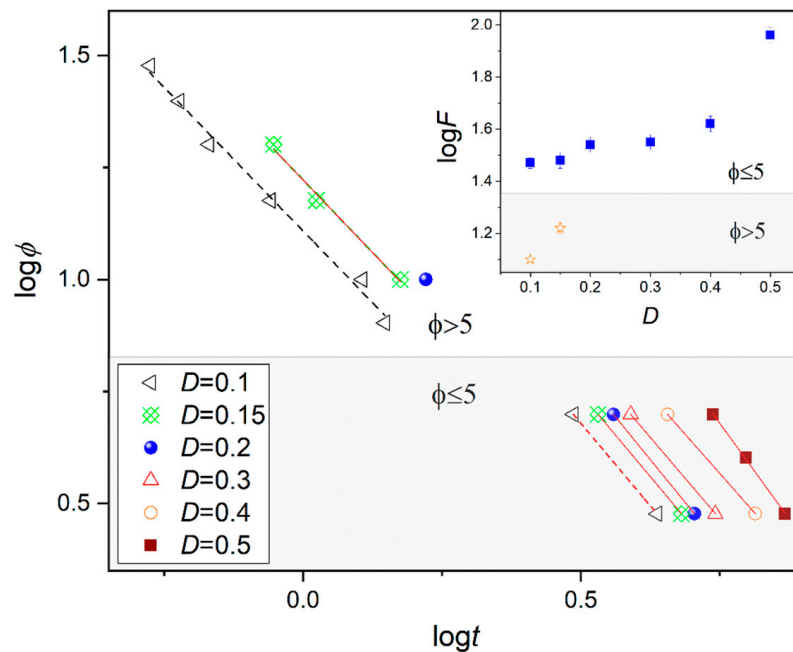


Figure 6. Plots of $\log\phi$ versus $\log t$ for a selected degree of crystallinity D during non-isothermal crystallization in the SmB phase of BBOA. The inset shows the dependence of $\log F$ on the crystallinity D .

3.3. Isothermal Melt Crystallization Kinetics of SmB_{cr} Studied by BDS

BDS is primarily intended to probe the response of polar substances to an external variable electric field. During the crystallization process, the number of fluctuating dipoles in a substance is gradually reduced, which is reflected as a decrease of the amplitude of the dielectric loss spectra $\varepsilon''(f)$ (see Figure 7a) and the dielectric strength ($\Delta\varepsilon = \varepsilon_s - \varepsilon_\infty$, where ε_s and ε_∞ are values of the real part ε' in the limit of low and high frequency, respectively). The evolution of the degree of crystallinity with time can be related to the change in normalized dielectric strength $\Delta\varepsilon_N$ as follows:

$$\varepsilon_N = \frac{\Delta\varepsilon(0) - \Delta\varepsilon(t)}{\Delta\varepsilon(0) - \Delta\varepsilon(\infty)} \quad (8)$$

where $\Delta\varepsilon(0)$, $\Delta\varepsilon(t)$ and $\Delta\varepsilon(\infty)$ are the values of the dielectric strength at, respectively, the beginning, the time t and at the end of the observation. The increase of a new crystalline fraction during the crystallization process can be described by Avrami model:

$$\Delta\varepsilon_N(t) = 1 - \exp(-K(t - t_0)^{n_A}) \quad (9)$$

where $K = k^{n_A}$ is a constant depending on the crystallization temperature and geometry of the sample, t_0 is the induction time, and n_A is the Avrami exponent. To determine the characteristic time of crystallization $\tau_{cryst} = K^{-1/n}$, defined as the time needed to achieve 63 % of the final crystallinity, Equation (9) was presented in the logarithmic form i.e., $\ln[-\ln(1 - \Delta\varepsilon_N)]$ versus $\ln(t)$; the result yielded a straight line, with n_A being the slope and $\ln K$ the intercept with the y-axis (Figure 7). The values of τ_{cryst} was designated from $\ln[-\ln(1 - \Delta\varepsilon_N)] = 0$ (see Figure 7c). The characteristic crystallization time (τ_{cryst}) increases with rising temperature (Figure 8), which suggests that the crystallization process is limited by the formation of nuclei. The activation energy ($E_a \approx 205$ kJ/mol) obtained for the isothermal experiment is consistent with that observed for a non-isothermal process with $\phi \leq 5$, accounting for experimental error; this suggests a continuous nucleation mechanism [10], which was also confirmed by POM studies. Hence, both isothermal crystallization in the temperature range 274 K to 281 K and non-isothermal process for $\phi \leq 5$ K/min is underpinned by a thermodynamic driving force. The n_A parameter (see Table 2), ranging from 2.8 to 2.3 with decreasing temperature, is reduced with respect

to the value expected for the homogeneous growth of the spherulitic nuclei ($n = 3$). Presumably, the reduction of crystal growth dimensionality observed for the non-isothermal experiment ($2.24 \leq n_o \leq 2.67$) is caused by a confinement effect, which is related to fact that the fractions of the layered SmB_{cr} are restricted by crystalline domains [21]. This effect was also found for crystallization of other materials in nanopores (two-dimensional confinement) [32] and for thin polymeric films (one-dimensional confinement) [33].

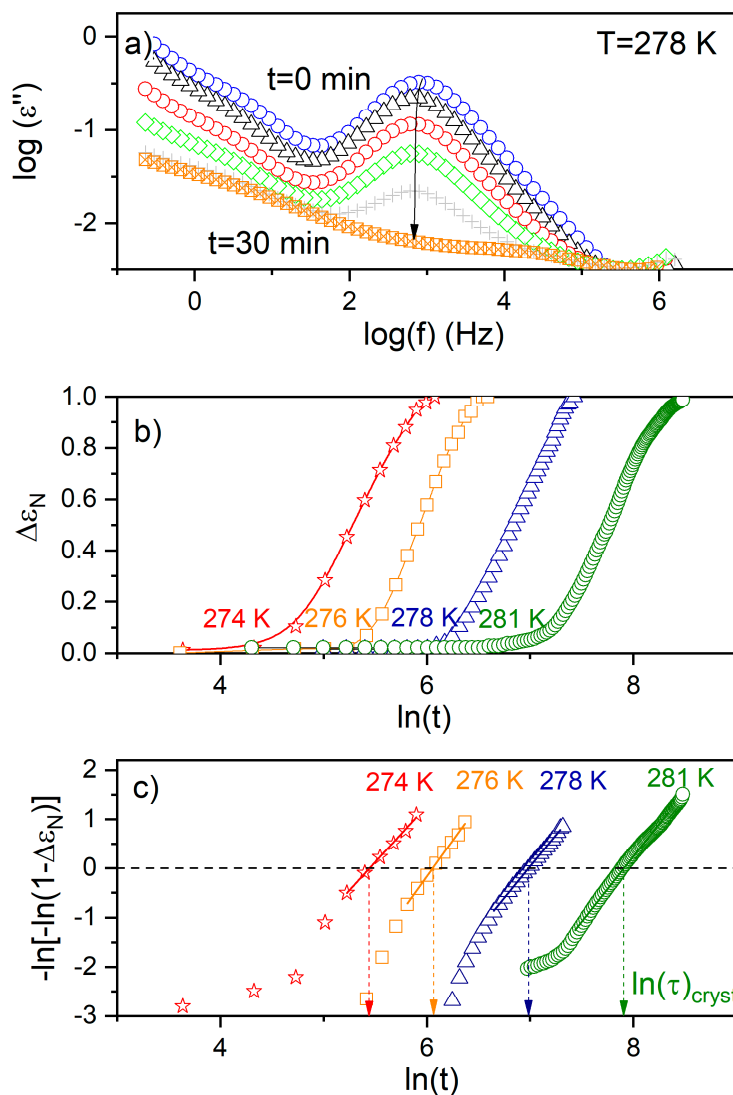


Figure 7. (a) The imaginary parts of the complex dielectric functions obtained upon isothermal crystallization of BBOA at 278 K. The arrow indicates the direction of changes in the loss spectra during the crystallization process. (b) Time evolution of the normalized dielectric strength ($\Delta\epsilon_N$) during isothermal crystallization of BBOA at 274 K, 276 K, 278 K and 276 K. (c) Avrami plot of $\Delta\epsilon_N(t)$ for the data presented in the panel (b).

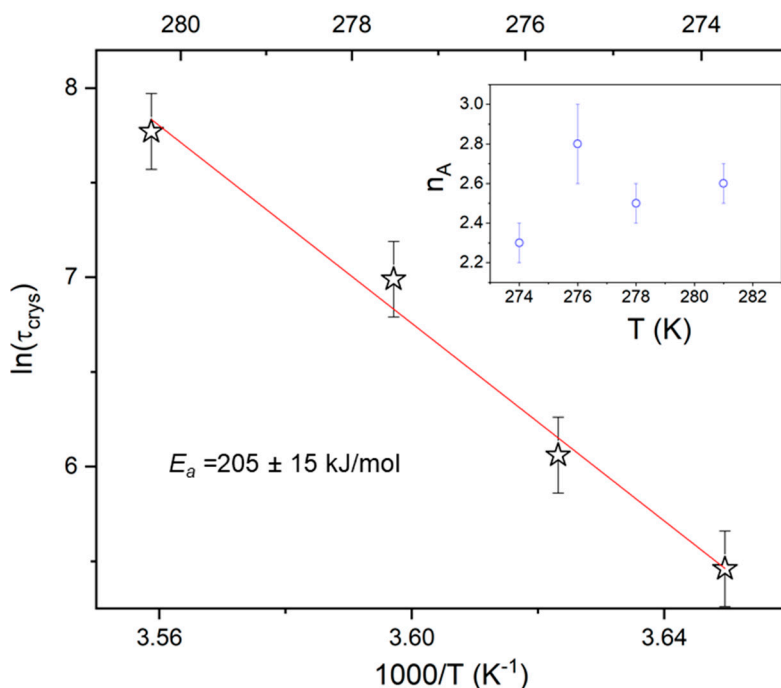


Figure 8. Temperature dependence of the characteristic crystallization time (τ_{crys}) for the isothermal melt crystallization form (SmB_{crys}) of BBOA. The inset presents the Avrami exponent n_A versus temperature.

Table 2. Parameters of isothermal melt crystallization kinetics of BBOA estimated by the Avrami model at different temperatures.

| T (K) | n_A | $\ln K$ | $\ln \tau_{cr}$ |
|---------|---------------|-----------------|-----------------|
| 274 | 2.3 ± 0.1 | -12.5 ± 0.2 | 5.5 ± 0.2 |
| 276 | 2.8 ± 0.1 | -17.3 ± 0.2 | 6.1 ± 0.2 |
| 278 | 2.5 ± 0.1 | -18.0 ± 0.2 | 6.9 ± 0.2 |
| 281 | 2.6 ± 0.2 | -19.7 ± 0.2 | 7.7 ± 0.2 |

4. Conclusions

The present study examined the kinetics of the non-isothermal and isothermal melt crystallization processes of SmB_{cr} in 4-n-butyloxybenzylidene-4'-n'-octylaniline (BBOA) by broadband dielectric spectroscopy, differential scanning calorimetry and polarized optical microscopy. Upon cooling, the SmB_{cr} phase of BBOA partially crystallizes and partially vitrifies; upon subsequent heating, the crystallization process is completed by cold crystallization. POM studies revealed that on heating, the degree of crystallinity changes according to the same Avrami curve observed for crystallization on cooling. Two crystallization mechanisms were revealed: (i) one based on thermodynamic forces at lower cooling rates ($3 \text{ K/min} \leq \phi \leq 5 \text{ K/min}$), with the energy barrier $E_a \approx 175$ kJ/mol and (ii) another controlled by diffusion which is associated with higher cooling rates ($5 \text{ K/min} > \phi \geq 30 \text{ K/min}$), with $E_a \approx 305$ kJ/mol.

This statement is supported by the results of analyses based on the Ozawa model and the approach proposed by Mo, which identified different parameters for the low and high cooling rates. The isothermal crystallization studied in the temperature range 274 K to 281 K is limited by the formation of nuclei. The activation energy ($E_a \approx 205$ kJ/mol) calculated for isothermal crystallization is comparable with that determined for the non-isothermal process taking place at $\phi \leq 5$ K/min, which suggests that both processes share the same mechanism. The parameters of crystal growth observed under isothermal ($2.3 \leq n_A \leq 2.8$) and non-isothermal conditions ($2.24 \leq n_o \leq 2.67$) show less dimensionality than that of the three-dimensional process. This is caused by the confinement of SmB_{cr} fractions in the layered sample by crystalline domains.

Author Contributions: M.J.-D.: conception of studies, BDS measurements and analysis of BDS data, analysis of kinetics of non-isothermal crystallization process based on DSC data and writing the manuscript. T.R.: POM measurements and analysis of POM data. E.J.-G.: DSC measurements and analysis of thermograms. All authors discussed the results and approved the final version of the manuscript.

Funding: M.J.-D. acknowledges the National Science Centre (Grant SONATA11: UMO-2016/21/D/ST3/01299) for financial support. E.J.G. acknowledges funding from the JINR research group and centers in Poland. (Studies of selected soft materials and compounds for hydrogen storage. Investigation of condensed matter by neutron scattering methods. Subject no: 04-4-1121-2015-2020.)

Conflicts of Interest: The authors declare no conflict of interest.

References

1. Ediger, M.D.; Harrowell, P.; Yu, L. Crystal growth kinetics exhibit a fragility-dependent decoupling from viscosity. *J. Chem. Phys.* **2008**, *128*, 034709. [[CrossRef](#)] [[PubMed](#)]
2. Tung, H.H.; Paul, E.L.; Midler, M.; McCauley, J.A. *Crystallization of Organic Compounds: An Industrial Perspective*; John Wiley & Sons, Inc.: Hoboken, New Jersey, USA, 2009; ISBN 978-0-471-46780-9.
3. Xue, D.; Li, K.; Liu, J.; Sun, C.; Chen, K. Crystallization and functionality of inorganic materials. *Mater. Res. Bull.* **2012**, *47*, 2838–2842. [[CrossRef](#)]
4. Gutzow, I.S.; Schmelzer, J.W.P. *The Vitreous State: Thermodynamics, Structure, Rheology, and Crystallization*, 2nd ed.; Springer: Berlin/Heidelberg, Germany, 1995; ISBN 978-3-642-34633-0.
5. Jackson, K.A. *Kinetic Processes*; Wiley-VCH Verlag GmbH & Co. KGaA: Weinheim, Germany, 2004; ISBN 9783527603893.
6. Szklarz, G.; Adrjanowicz, K.; Paluch, M. Cooling-Rate versus Compression-Rate Dependence of the Crystallization in the Glass-Forming Liquid, Propylene Carbonate. *Cryst. Growth Des.* **2018**, *18*, 2538–2544. [[CrossRef](#)]
7. Sanz, A.; Niss, K. Coupling between Molecular Mobility and Kinetics of Crystal Growth in a Hydrogen-Bonded Liquid. *Cryst. Growth Des.* **2017**, *17*, 4628–4636. [[CrossRef](#)]
8. Swallen, S.F.; Ediger, M.D. Self-diffusion of the amorphous pharmaceutical indomethacin near T_g. *Soft Matter* **2011**, *7*, 10339–10344. [[CrossRef](#)]
9. Descamps, M.; Dudognon, E. Crystallization from the amorphous state: Nucleation-growth decoupling, polymorphism interplay, and the role of interfaces. *J. Pharm. Sci.* **2014**, *103*, 2615–2628. [[CrossRef](#)]
10. Zhou, D.; Zhang, G.G.Z.; Law, D.; Grant, D.J.W.; Schmitt, E.A. Thermodynamics, molecular mobility and crystallization kinetics of amorphous griseofulvin. *Mol. Pharm.* **2008**, *5*, 927–936. [[CrossRef](#)]
11. Schmelzer, J.W.P.; Abyzov, A.S. Crystallization of glass-forming liquids: Specific surface energy. *J. Chem. Phys.* **2016**, *145*, 064512. [[CrossRef](#)]
12. Pełka, R.; Yamamura, Y.; Jasiurkowska, M.; Massalska-Arodź, M.; Saito, K. Rich polymorphism in 4-propyl-4'-thiocyanato-1,1'-biphenyl (3TCB) revealed by adiabatic calorimetry. *Liq. Cryst.* **2008**, *35*, 179–186. [[CrossRef](#)]
13. Massalska-Arodź, M.; Williams, G.; Smith, I.K.; Conolly, C.; Anthony Aldridge, G.; Dabrowski, R. Molecular dynamics and crystallization behaviour of isopentyl cyanobiphenyl as studied by dielectric relaxation spectroscopy. *J. Chem. Soc. Faraday Trans.* **1998**, *94*, 387–394. [[CrossRef](#)]
14. Massalska-Arodź, M.; Williams, G.; Thomas, D.K.; Jones, W.J.; Dabrowski, R. Molecular Dynamics and Crystallization Behavior of Chiral Isooctyloxycyanobiphenyl as Studied by Dielectric Relaxation Spectroscopy. *J. Phys. Chem. B* **1999**, *103*, 4197–4205. [[CrossRef](#)]
15. Rozwadowski, T.; Massalska-Arodź, M.; Kolek, .; Grzybowska, K.; Bąk, A.; Chłędowska, K. Kinetics of Cold Crystallization of 4-Cyano-3-fluorophenyl 4-Butylbenzoate (4CFPB) Glass Forming Liquid Crystal. I. Nonisothermal Process As Studied by Microscopic, Calorimetric, and Dielectric Methods. *Cryst. Growth Des.* **2015**, *15*, 2891–2900. [[CrossRef](#)]
16. Jasiurkowska-Delaporte, M.; Rozwadowski, T.; Dmochowska, E.; Juszyńska-Gałązka, E.; Kula, P.; Massalska-Arodź, M. Interplay between Crystallization and Glass Transition in Nematic Liquid Crystal 2,7-Bis(4-pentylphenyl)-9,9-diethyl-9H-fluorene. *J. Phys. Chem. B* **2018**, *122*, 10627–10636. [[CrossRef](#)]
17. Georgopoulos, D.; Kriptou, S.; Argyraki, E.; Kyritsis, A.; Pissis, P. Study of Isothermal Crystallization Kinetics of 5CB with Differential Scanning Calorimetry and Broadband Dielectric Spectroscopy. *Mol. Cryst. Liq. Cryst.* **2015**, *611*, 197–207. [[CrossRef](#)]

18. Mastrangelo, J.C.; Blanton, T.N.; Chen, S.H. Crystallization upon thermal annealing of a glass-forming liquid crystal in the nematic regime. *Appl. Phys. Lett.* **1995**, *66*, 2212–2214. [[CrossRef](#)]
19. Juszyńska, E.; Jasiurkowska, M.; Massalska-Arodź, M.; Takajo, D.; Inaba, A. Phase Transition and Structure Studies of a Liquid Crystalline Schiff-Base Compound (4O.8). *Mol. Cryst. Liq. Cryst.* **2011**, *540*, 127–134. [[CrossRef](#)]
20. Dierking, I. *Textures of Liquid Crystals*; Wiley-VCH Verlag GmbH & Co. KGaA: Weinheim, Germany, 2003; ISBN 3527307257.
21. Jasiurkowska-Delaporte, M.; Napolitano, S.; Leys, J.; Juszyńska-Gałązka, E.; Wübbenhorst, M.; Massalska-Arodź, M. Glass Transition Dynamics and Crystallization Kinetics in the Smectic Liquid Crystal 4-n-Butyloxybenzylidene-4'-n'-octylaniline (BBOA). *J. Phys. Chem. B* **2016**, *120*, 12160–12167. [[CrossRef](#)] [[PubMed](#)]
22. Górecka, E.; Chen, L.; Pyżuk, W.; Krówczyński, A.; Kumar, S. X-ray studies of the hexatic phase in liquid crystals with a crystal-B–hexatic-B–smectic-A phase sequence. *Phys. Rev. E* **1994**, *50*, 2863–2867. [[CrossRef](#)]
23. Rao, N.V.S.; Potukuchi, D.M.; Pisipati, V.G.K.M. Phase Transitions in N(p-n-Bu toxybenzylidene) p-n-Alkyl Anilines: Density and Refractive Index Studies. *Mol. Cryst. Liq. Cryst.* **1991**, *196*, 71–87. [[CrossRef](#)]
24. Haines, P.J. *Thermal Methods of Analysis: Principles, Applications and Problems*; Springer: Dordrecht, Netherlands, 1995; ISBN 978-0751400502.
25. Suzuki, Y.; Yamamura, Y.; Sumita, M.; Yasuzuka, S.; Saito, K. Neat Liquid Consisting of Hydrogen-Bonded Tetramers: Dicyclohexylmethanol. *J. Phys. Chem. B* **2009**, *113*, 10077–10080. [[CrossRef](#)]
26. Henderson, D.W. Thermal analysis of non-isothermal crystallization kinetics in glass forming liquids. *J. Non-Cryst. Solids* **1979**, *30*, 301–315. [[CrossRef](#)]
27. Kissinger, H.E. Variation of Peak Temperature With Heating Rate In Differential Thermal Analysis. *J. Res. Natl. Bur. Stand. (1934)* **1956**, *57*, 217–221. [[CrossRef](#)]
28. Augis, J.A.; Bennett, J.E. Calculation of the Avrami parameters for heterogeneous solid state reactions using a modification of the Kissinger method. *J. Therm. Anal. Calorim.* **1978**, *13*, 283–292. [[CrossRef](#)]
29. Ozawa, T. Kinetics of non-isothermal crystallization. *Polymer* **1971**, *12*, 150–158. [[CrossRef](#)]
30. Liu, Y.; Wang, L.; He, Y.; Li, S. Nonisothermal Crystallization Kinetics of Poly(b-hydroxybutyrate). *J. Polym. Sci. Part B Polym. Phys.* **1998**, *36*, 1305–1312.
31. Liu, T.; Mo, Z.; Wang, S.; Zhang, H. Nonisothermal Melt and Cold Crystallization Kinetics of Poly(Ary1 Ether Ether Ketone Ketone). *Polym. Eng. Sci.* **1997**, *33*, 568–575. [[CrossRef](#)]
32. Kołodziejczyk, K.; Tarnacka, M.; Kamińska, E.; Dulski, M.; Kamiński, K.; Paluch, M. Crystallization Kinetics under Confinement. Manipulation of the Crystalline Form of Salol by Varying Pore Diameter. *Cryst. Growth Des.* **2016**, *16*, 1218–1227. [[CrossRef](#)]
33. Napolitano, S.; Wübbenhorst, M. Slowing Down of the Crystallization Kinetics in Ultrathin Polymer Films: A Size or an Interface Effect? *Macromolecules* **2006**, *39*, 5967–5970. [[CrossRef](#)]

